

**Ground state of spin-1 Bose-Einstein condensates with spin-orbit coupling in a Zeeman field**L. Wen,<sup>1</sup> Q. Sun,<sup>1,\*</sup> H. Q. Wang,<sup>2</sup> A. C. Ji,<sup>3,†</sup> and W. M. Liu<sup>1</sup><sup>1</sup>*Beijing National Laboratory for Condensed Matter Physics, Institute of Physics, Chinese Academy of Sciences, Beijing 100190, China*<sup>2</sup>*School of Statistics and Mathematics, Yunnan University of Finance and Economics, Kunming, Yunnan Province, 650221, China*<sup>3</sup>*Center of Theoretical Physics, Department of Physics, Capital Normal University, Beijing 100048, China*

(Received 14 August 2012; published 3 October 2012)

We systematically investigate the weakly trapped spin-1 Bose-Einstein condensates with spin-orbit coupling in an external Zeeman field. We find that the mean-field ground state favors either a magnetized standing-wave phase or plane-wave phase when the strength of the Zeeman field is below a critical value related to the strength of spin-orbit coupling. The Zeeman field can induce a phase transition between standing-wave and plane-wave phases, and we determine the phase boundary analytically and numerically. The magnetization of these two phases responds to the external magnetic field in a very unique manner: the linear Zeeman effect magnetizes the standing-wave phase along the direction of the magnetic field, but the quadratic Zeeman effect demagnetizes the plane-wave phase. When the strength of Zeeman field surpasses the critical value, the system is completely polarized to a ferromagnetic state or polar state with zero momentum.

DOI: [10.1103/PhysRevA.86.043602](https://doi.org/10.1103/PhysRevA.86.043602)

PACS number(s): 03.75.Mn, 05.30.Jp, 67.85.Fg, 67.85.Jk

**I. INTRODUCTION**

Spin-orbit coupling, which is generally referred to the coupling of a particle's spin with its degree of motion in quantum physics, is responsible for many fundamental physical phenomena in quantum systems, such as the spin Hall effects and topological insulators [1]. Recently, with the pioneering experimental realization of an artificial Abelian or non-Abelian gauge potential in neutral atoms [2,3], an effective spin-orbit coupling has been created in spinor Bose-Einstein condensates (BEC) by dressing two atomic spin states with a pair of lasers [4–8]; a result that has attracted a great deal of attention in the condensed matter community. In particular, the spin-orbit coupling effects can give rise to many intriguing exotic ground states in an interacting ultracold spinor Bose gas, such as the plane-wave (PW), standing-wave (SW), triangular-lattice, and square-lattice phases [9–29]. Moreover, in pseudo-spin-1/2 BEC, the combined effects of Rashba spin-orbit coupling and rotating trap can also produce some unusual topological patterns including the skyrmion and giant vortex [30–32].

Generally, without spin-orbit coupling, a spinor BEC exhibits a variety of magnetic phenomena. Taking the spin-1 BEC as an example, the mean-field ground state can be a ferromagnetic, antiferromagnetic, or polar state [33]. Which type of these phases is favored by the ground state depends on the spin-dependent atomic interaction. Interestingly, an external Zeeman field can transform these phases into each other by tuning their magnetization and results in a rich ground state phase diagram [34,35]. For example, a broken-axisymmetry state can emerge as an intermediate phase in the transition between the ferromagnetic and polar phases. Such phase transitions reflect that the magnetic system responds to the external magnetic field in a very unique manner. So the

application of an external magnetic field provides a powerful way to experimentally manipulate the magnetic behaviors of a spinor BEC [34].

However, when the spin-orbit coupling is taken into account, the situation changes. The ground state of spin-1 BEC now could be a PW phase occupying a single momentum state or a SW phase formed by the coherent superposition of two plane waves with opposite momentum [10], and these two phases possess different magnetic properties. So it is interesting and important to study the effects of an external Zeeman field on these phases, which is the main contents of this work. To make this point more transparent, in this paper, we consider a weakly trapped two-dimensional spin-1 BEC with Rashba spin-orbit coupling in a Zeeman field. We find that, if the Zeeman field is not too strong, the system is in a magnetized SW phase or PW phase, and the phase boundary immerses into the SW phase due to the competition between Zeeman effects and spin-dependent atomic interaction. The Zeeman field modulates the magnetization of these two phases in different manners. For example, the linear Zeeman field magnetizes the SW phase, but the quadratic one demagnetizes the PW phase. While the strength of the Zeeman field surpasses a critical value determined by the strength of spin-orbit coupling, the system is completely polarized to either a ferromagnetic state or a polar state with zero momentum.

This paper is organized as follows: We first give the model in Sec. II and discuss the single-particle ground state in Sec. III. By using the variational approximation method and the numerical simulation, we give the phase diagram of the mean-field ground state and study the effects of a Zeeman field on the magnetization of this system in Sec. IV. Finally, we conclude our results in Sec. V.

**II. THE MODEL**

We consider a quasi-two-dimensional spin-1 BEC with Rashba type spin-orbit coupling in the Zeeman field, where the particle's spin couples its degree of motion in the  $xy$  plane. In the mean-field approximation, the Gross-Pitaevskii energy

\*sunqing@iphy.ac.cn

†andrewjee@sina.com

functional of such a system is of the form

$$\begin{aligned}
E = \int dr \left\{ \sum_m \psi_m^* \left[ -\frac{\hbar^2 \nabla^2}{2M} - pm + qm^2 \right] \psi_m \right. \\
+ \frac{\hbar\kappa}{M} [\psi_1^* (-i\partial_x - \partial_y) \psi_0 + \psi_0^* (-i\partial_x - \partial_y) \psi_{-1} + \text{H.c.}] \\
\left. + \frac{c_0}{2} n^2 + \frac{c_2}{2} [(n_1 - n_{-1})^2 + 2|\psi_1^* \psi_0 + \psi_0^* \psi_{-1}|^2] \right\}, \quad (1)
\end{aligned}$$

where  $m = 1, 0, -1$  and the density distribution of the component  $m$  reads  $n_m = |\psi_m|^2$  with the condensation wave function  $\psi_m$ , thus the total atomic density is  $n = \sum_m n_m$ . For the spin-orbit coupling term, we consider the symmetric Rashba case  $\kappa_x = \kappa_y = \kappa$ , where  $\kappa$  is the strength of spin-orbit coupling related to the wavelength of Raman lasers [4]. For the interaction terms,  $c_0$  and  $c_2$  are the interaction parameters which depend on two-body  $s$ -wave scattering lengths  $a_0$  and  $a_2$  for total spin 0, 2:  $c_0 = 4\pi\hbar^2 N(a_0 + 2a_2)/(3M)$  and  $c_2 = 4\pi\hbar^2 N(a_2 - a_0)/(3M)$  with the atomic mass  $M$  and total atomic number  $N$ . To avoid the collapse of the BEC under attractive interaction,  $c_0$  is assumed to be nonnegative throughout this paper. Moreover,  $p$  and  $q$  represent the strength of the linear and quadratic Zeeman effects, respectively. The strengths are determined by the magnetic field  $B$  such that  $p = -g\mu_B B$  and  $q = \mu_B^2 B^2/(4E_{hfs})$ , where  $g$  is the Landé hyperfine factor,  $\mu_B$  is the Bohr magneton, and  $E_{hfs}$  is the hyperfine splitting. For the sake of simplicity, the external magnetic field is assumed to be applied in the  $z$  direction, and the values of  $p$  and  $q$  are taken to be nonnegative constants.

### III. SINGLE-PARTICLE GROUND STATE

To gain some intuition, it is instructive to start our investigations with the noninteracting Hamiltonian in the homogeneous case. The single-particle Hamiltonian preserves the symmetries of simultaneous spin and space rotations around the direction of the applied magnetic field. The group describing such symmetries is  $SO(2)$  which has discrete subgroups  $C_{nz}$  [26]. The single-particle ground state in absence of the external magnetic field is not unique so that it is infinitely degenerate along a circular ring with radius  $k_\perp = (k_x^2 + k_y^2)^{1/2} = \sqrt{2}\kappa/\hbar$  in two-dimensional momentum space [10,27], where  $k_x$  and  $k_y$  are the components of momentum along  $x$  and  $y$  directions, respectively. In the presence of the Zeeman field, we first consider two simple cases in which the linear and quadratic Zeeman effects are considered separately. Their combined effects will be considered later.

Due to the typical Rashba spin-orbit coupling, the spin degeneracy of spinor bosons is lifted by the spin-orbit coupling [10], the single-particle energy spectrum splits into three energy branches with different helicity in momentum space:

$$L : E_0 = E_{\mathbf{k}}, \quad E_{\pm} = E_{\mathbf{k}} \pm \sqrt{p^2 + \frac{4\kappa^2}{M}} E_{\mathbf{k}}, \quad (2a)$$

$$Q : E_0 = E_{\mathbf{k}} + q, \quad E_{\pm} = E_{\mathbf{k}} + \frac{1}{2}q \pm \frac{1}{2}\sqrt{q^2 + \frac{16\kappa^2}{M}} E_{\mathbf{k}}, \quad (2b)$$

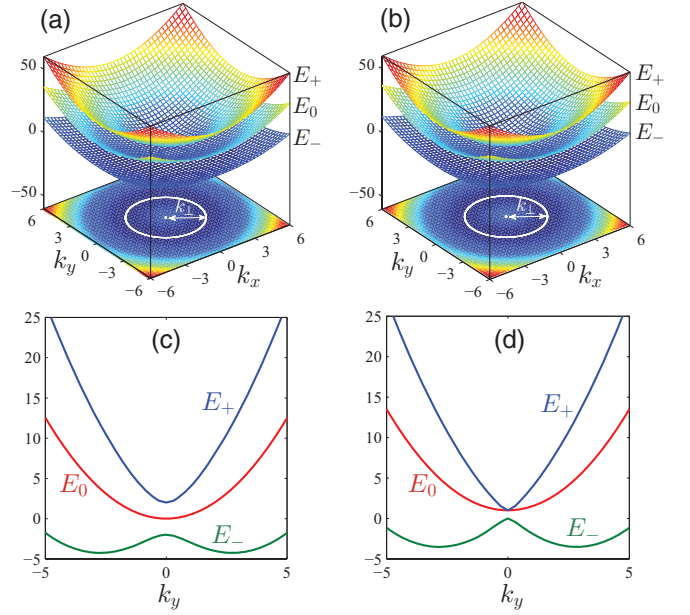


FIG. 1. (Color online) (a) Single-particle energy spectrum in linear Zeeman field with  $p = 2$ . (b) Single-particle energy spectrum in quadratic Zeeman field with  $q = 1$ . Note that the figures in the bottom of (a) and (b) represent the projections of  $E_-$  on the  $k_x$ - $k_y$  plane, and the white circular rings are the momentum of infinitely degenerate ground states in  $E_-$ . Furthermore, to clarify the energy gap between these energy branches, panels (c) and (d) plot the energy spectrums at  $k_x = 0$ . In all the figures, the other parameters are the same:  $M = \hbar = 1$  and  $\kappa = 2$ .

where  $L$  and  $Q$  represent the energy spectrums in linear and quadratic Zeeman fields, respectively.  $E_{\mathbf{k}} = \hbar^2 k_\perp^2/(2M)$  is the kinetic energy of a free particle. The subscript  $\pm$  denotes the helicity branches of spin parallel or antiparallel to the wave vector, respectively. As shown in Fig. 1, the single-particle ground states are in the negative helicity branch  $E_-$  with the momentums  $k_\perp = (\frac{2\kappa^2}{\hbar^2} - \frac{M^2 p^2}{2\hbar^2 \kappa^2})^{1/2}$  in the linear Zeeman field and  $k_\perp = (32\kappa^4 - 2q^2 M^2)^{1/2}/(4\hbar\kappa)$  in the quadratic Zeeman field, respectively. The corresponding single-particle eigenstates are given by

$$\Psi_{\mathbf{k}} = \begin{pmatrix} \alpha_1 \\ -\alpha_0 e^{i\theta} \\ \alpha_{-1} e^{i2\theta} \end{pmatrix} e^{i\mathbf{k}\cdot\mathbf{r}}, \quad (3)$$

where  $\theta = \arctan(k_y/k_x)$ , and the coefficients  $\alpha_m$  satisfying  $\sum_m \alpha_m^2 = 1$  are

$$L : \alpha_1 = \frac{2\kappa^2 + Mp}{4\kappa^2}, \quad \alpha_{-1} = \frac{2\kappa^2 - Mp}{4\kappa^2}, \quad \alpha_0 = \sqrt{2\alpha_1\alpha_{-1}}, \quad (4a)$$

$$Q : \alpha_1 = \alpha_{-1} = \frac{\sqrt{4\kappa^2 - Mq}}{4\kappa}, \quad \alpha_0 = \frac{\sqrt{2}\sqrt{4\kappa^2 + Mq}}{4\kappa}, \quad (4b)$$

which shows that the three spin components are coupled strongly in this energy branch.

From the results above, on the one hand, the Zeeman effects shift the momentum of ground state compared to the

case of no external magnetic field. All the single-particle states with same momentum  $k_{\perp}$  but different azimuthal angle in two-dimensional momentum space are degenerate ground states; namely, the single-particle ground states are infinitely degenerate along a circular ring with the radius  $k_{\perp}$  shown in Figs. 1(a) and 1(b). Moreover, since the momentum of the ground state should be real, we have noted that there exists two additional restraint conditions  $p \leq 2\kappa^2/M$  and  $q \leq 4\kappa^2/M$ . In particular, if the strength of the linear or quadratic Zeeman effect takes the maximal critical value, the circular ring of momentum in infinitely degenerate ground states shrinks to the zero-momentum point [the center of the ring shown in Figs. 1(a) and 1(b)] so that the system is polarized to a nondegenerate ground state. On the other hand, at the point of  $k_{\perp} = 0$ , the presence of the Zeeman field can open an energy gap between these energy branches, as shown in Figs. 1(c) and 1(d). In a linear Zeeman field, the gaps between adjacent energy branches are  $\Delta_{+0} = E_{+} - E_0 = p$  and  $\Delta_{0-} = E_0 - E_{-} = p$ . While the quadratic Zeeman field only opens the gap  $\Delta_{+-} = \Delta_{0-} = q$  between the energy branches  $E_{+}$  (or  $E_0$ ) and  $E_{-}$ , it is gapless between  $E_{+}$  and  $E_0$ . These facts demonstrate that the linear and quadratic Zeeman effects play different roles in affecting the structure of the single-particle energy spectrum.

Let us now consider the combination effect of the linear and quadratic Zeeman terms. For simplification, we just give the lower-energy branch with negative helicity denoted as  $E_{-}$  in the single-particle energy spectrums as follows:

$$E_{-} = E_{\mathbf{k}} + \frac{2q}{3} + 2\Delta^{\frac{1}{3}} \cos\left(\beta + \frac{2\pi}{3}\right) \quad (5)$$

where  $\Delta = (\Gamma^3/27)^{1/2}$  with  $\Gamma = 4\kappa^2 E_{\mathbf{k}}/M + p^2 + q^2/3$ ,  $\beta = \frac{1}{3} \arccos(-\frac{\Theta}{2\Delta})$  with  $\Theta = \frac{2}{27}q(18\kappa^2 E_{\mathbf{k}}/M - 9p^2 + q^2)$ . We have to point out that the energy in Eq. (5) is a real quantity under the constrained condition  $|\frac{\Theta}{2}| < \Delta$  related to a real quantity  $\beta$ . But it can be checked that the constrained condition is always satisfied for arbitrary  $p$  and  $q$ . Since the expression of the energy spectrum in Eq. (5) is very complex, it is impossible to analytically solve the momentum of the single-particle ground state and derive the coefficient  $\alpha_m$  of the corresponding eigenstates in Eq. (3), so we plot these quantities in Fig. 2 by seeking the minimal value of energy [Eq. (5)] numerically. It

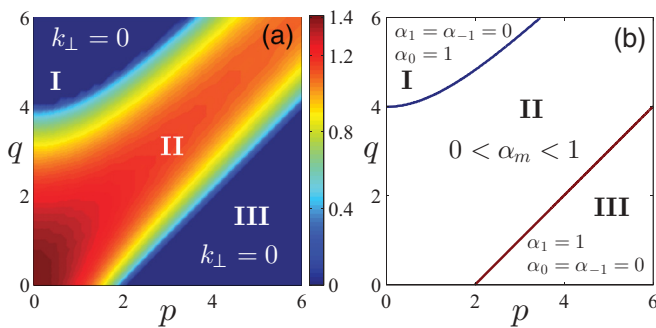


FIG. 2. (Color online) (a) Change in momentum of single-particle ground state with the linear and quadratic Zeeman effects. (b) Change in coefficients  $\alpha_m$  of single-particle eigenstates in Eq. (3) with the linear and quadratic Zeeman effects. In both (a) and (b), the parameters are  $\kappa = 1$  and  $\hbar = M = 1$ .

can be clearly seen that the quadratic Zeeman effect dominates in region I, but the linear Zeeman effect dominates in region III. In both regions I and III, the momentum of the single-particle ground state is zero, and the corresponding coefficients  $\alpha_m$  in the single-particle eigenstate are  $(0, 1, 0)^T$  and  $(1, 0, 0)^T$ , respectively. These results imply that the system is polarized by the magnetic field in both regions I and III. While in region II, the coefficient satisfies  $0 < \alpha_m < 1$ , and the momentum of the ground state is nonzero so that the single-particle ground states are infinitely degenerate along a circular ring with radius  $k_{\perp}$  in momentum space. Furthermore, the boundary between the regions II and III can be analytically fixed; that is,  $q/3 - p - 2\sqrt[3]{\Delta} \cos(\beta + \frac{2\pi}{3}) = 0$ .

#### IV. MEAN-FIELD GROUND STATE IN EXTERNAL ZEEMAN FIELD

For the spin-1 BEC with Rashba spin-orbit coupling, the interaction effects in the absence of a Zeeman field have been investigated extensively [10,26,27]. In the homogeneous case, the mean-field ground state favors either the PW for  $c_2 < 0$  or the SW for  $c_2 > 0$ ; the former is a ferromagnetic state, but the latter is a polar state [10]. These phases spontaneously break the rotational symmetry about the  $z$  direction despite the fact that the Hamiltonian is axisymmetric. In particular, these two different phases are degenerate for  $c_2 = 0$ . Now the point is that, if a Zeeman field along the  $z$  direction is turned on, we are inquisitive about whether an external magnetic field can essentially change the phase diagram of the mean-field ground state for a spin-orbit coupled spin-1 BEC. How does the external magnetic field affect the magnetization of the ground state? The investigation of the unique features of these problems is the primary purpose of this section.

In two-dimensional homogeneous system, the interacting Hamiltonian preserves the symmetries of the single-particle Hamiltonian, and the atomic interactions can couple different single-particle states so that the ground state, preserving symmetry  $C_{nz}$ , can be approximately described by the linear superposition of single-particle eigenstates on the degenerate momentum ring,  $\Psi = \sum_n \mathcal{A}_n \Psi_{\mathbf{k}}$  with  $\mathcal{A}_n$  satisfying  $\sum_n |\mathcal{A}_n|^2 = 1$ , where  $n$  is a nonnegative integer [10,26]. By substituting the ansatz into Eq. (1) to compute the energy, we find that these high-symmetry states with  $n \geq 3$  are energetically unfavored by ground state which can be verified by our numerical results. Thus, this fact motivates us to choose the following ansatz for clarifying the phase diagram of the mean-field ground state and developing a simple physical understanding in the following discussions:

$$\Psi = \mathcal{A}\Psi_{\mathbf{k}} + \mathcal{B}\Psi_{-\mathbf{k}}, \quad (6)$$

where  $\Psi_{\mathbf{k}}$  and  $\Psi_{-\mathbf{k}}$  are two counterpropagating plane waves in Eq. (3), and the superposition coefficients  $\mathcal{A}$  and  $\mathcal{B}$  are real constants satisfying the normalization condition  $\mathcal{A}^2 + \mathcal{B}^2 = 1$  under  $\sum_m \int |\psi_m|^2 dr = 1$ .

By inserting the ansatz into the mean-field energy functional [Eq. (1)], we can obtain the energy expression as a function of the parameter  $\mathcal{A}$ :

$$E[\mathcal{A}] = \xi(\mathcal{A}^4 - \mathcal{A}^2) + \text{const}, \quad (7)$$

where  $\xi = [2\alpha_0^2(\alpha_1^2 + 6\alpha_1\alpha_{-1} + \alpha_{-1}^2) - (\alpha_1^2 - \alpha_{-1}^2)^2]c_2 - (\alpha_1^2 - \alpha_0^2 + \alpha_{-1}^2)c_0$ . Note that some constants unrelated to  $\mathcal{A}$  in Eq. (7) are omitted. We can immediately determine the phase diagram of the mean-field ground state by minimizing the energy with respect to  $\mathcal{A}$ : (i) The PW phase with  $\mathcal{A} = 0$  and  $\mathcal{B} = 1$  if  $\xi < 0$ . (ii) The SW phase with  $\mathcal{A} = \mathcal{B} = 1/\sqrt{2}$  if  $\xi > 0$ . In particular, these two phases are degenerate when  $\xi = 0$ . These results demonstrate that the external magnetic field shifts the phase boundary from  $c_2 = 0$  to  $\xi(c_2, p, q) = 0$  due to the competition between the Zeeman effects and the spin-dependent interaction.

To further explore the physics behind this, in what follows we perform a detailed analysis of the phase diagram of the ground state and investigate the effects of an external magnetic field on the magnetic behavior of this system. We first consider the linear and quadratic Zeeman effects separately. Their combined effects will be considered afterward.

### A. Phase diagram and magnetic behavior of ground state in linear or quadratic Zeeman field

In the linear or quadratic Zeeman field, the phase boundaries are  $\xi = (2 - M^2 p^2/\kappa^4)c_2 + \frac{M^4 p^4}{16\kappa^8}(c_2 - c_0)$  or  $\xi = 2c_2 - \frac{M^2 q^2}{16\kappa^4}(2c_2 + c_0)$ , respectively. In the parameter spaces  $(c_2, p)$  and  $(c_2, q)$ , the corresponding phase diagrams of the mean-field ground state are shown in Fig. 3. We observe that the SW phase only exists for the case  $c_2 > 0$ ; the region of which is less than the region occupied by the PW in the  $c_2$ - $p$  or  $c_2$ - $q$  plane. More importantly, the external magnetic field can induce the phase transition from the SW to PW when the strength of the magnetic field surpasses the critical value  $p_0 = 2\kappa^2\{[(2c_2^2 + 2c_2c_0)^{1/2} - 2c_2]/[M^2(c_0 - c_2)]\}^{1/2}$  on the phase boundary for the linear Zeeman effect (or  $q_0 = 4\kappa^2\{2c_2/[(c_0 + 2c_2)M^2]\}^{1/2}$  for the quadratic Zeeman effect), where we require  $c_0 \gg c_2$  in accordance with real experiments. In particular, if the strength of the linear (or quadratic) Zeeman effect attain the critical values  $p_m = 2\kappa^2/M$  (or  $q_m = 4\kappa^2/M$ ), the system can be polarized by the magnetic

field so that all the atoms will occupy the state  $\psi_1$  (or  $\psi_0$ ) with zero momentum, in which the ground state is ferromagnetic state (or polar state).

Based on the coupled Gross-Pitaevskii equations, we have checked all the analytical predictions by using the imaginary time evolution method to numerically look for the ground-state solutions which can minimize the mean-field energy. A very weak isotropic harmonic potential is included in our numerical simulation, but it does not change the results in the homogeneous case. As shown in Fig. 3, these analytical predictions given by the ansatz in Eq. (6) agree with the numerical results very well, which demonstrates that the excellent ansatz in Eq. (6) captures all the fundamental physics. Moreover, we would like to point out that, although  $p$  and  $q$  should satisfy the constrained conditions  $p \leq 2\kappa^2/M$  and  $q \leq 4\kappa^2/M$  in analytical predictions, our numerical results demonstrate that the mean-field ground states are still the completely polarized ferromagnetic or polar states for  $p > 2\kappa^2/M$  and  $q > 4\kappa^2/M$  as shown in Fig. 3.

Next, we investigate how the external Zeeman field affects the magnetization of this system. In general, the magnetization for spin-1 BEC is defined as  $\mathcal{M} = (\mathcal{M}_x^2 + \mathcal{M}_y^2 + \mathcal{M}_z^2)^{1/2}$  with  $\mathcal{M}_\mu = \sum_{mn} \int \psi_m^*(\sigma_\mu)_{mn} \psi_n dx dy$  being the component of magnetization along the directions  $\mu = x, y, z$ , where the subscripts  $m, n = 1, 0, -1$ , and  $\sigma_\mu$  represents the  $3 \times 3$  spin matrix [35]. We first use the ansatz in Eq. (6) to analytically compute the magnitude of magnetization for the cases of  $c_2 < 0$  and  $c_2 > 0$ , respectively. The results are listed in Table I. It can be seen that the SW and PW phases respond to the external magnetic field in very different manners. In a linear Zeeman field, the ground state is PW when  $c_2 < 0$ ; the magnitude of magnetization always remains invariant regardless of the external magnetic field. For the case of  $c_2 > 0$ , the system is initially in the SW phase if  $p < p_0$ , the magnitude of magnetization increases linearly from zero. When  $p > p_0$ , the system has transformed into PW and the magnitude of magnetization undergoes a discontinuous sudden transition from  $\mathcal{M} = Mp_0/(2\kappa^2)$  to  $\mathcal{M} = 1$ . In a quadratic Zeeman field, the magnitude of the magnetization of PW for  $c_2 < 0$  decays quadratically from  $\mathcal{M} = 1$  to  $\mathcal{M} = 0$  with increasing strength of the magnetic field, which implies that the quadratic Zeeman effect demagnetizes the PW. However, for the case of  $c_2 > 0$ , the quadratic Zeeman effect can not change the magnetization of the SW phase if  $q < q_0$ . When the strength of magnetic field surpasses the critical value  $q_0$ , the system suddenly possesses magnetization

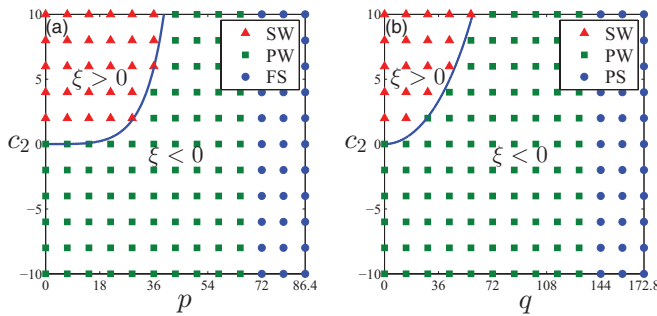


FIG. 3. (Color online) (a) Phase diagram of mean-field ground state in linear Zeeman field. (b) Phase diagram of mean-field in quadratic Zeeman field. The red triangles and green squares respectively denote the SW and PW phases given by numerical results, and the blue line is the phase boundary  $\xi = 0$  between these two phases. The blue circles represent the zero-momentum ferromagnetic state (FS) in (a) and the zero-momentum polar state (PS) in (b), respectively. The other parameters in both the figures are  $c_0 = 100$ ,  $M = 1$  and  $\kappa = 6$ .

TABLE I. Expressions of magnetization in linear and quadratic Zeeman fields, respectively. For  $c_2 > 0$ , the ground state during  $p < p_0$  or  $q < q_0$  is the SW phase, but it is the PW phase for  $p > p_0$  or  $q > q_0$ . For  $c_2 < 0$ , the ground state is always PW for an arbitrary  $p$  or  $q$ .

	Linear Zeeman field	Quadratic Zeeman field
$c_2 < 0$	$\mathcal{M}_{\text{PW}} = 1$	$\mathcal{M}_{\text{PW}} = \frac{\sqrt{16\kappa^4 - M^2 q^2}}{4\kappa^2}$
$c_2 > 0$	$\mathcal{M}_{\text{SW}}^{p < p_0} = \frac{Mp}{2\kappa^2}$	$\mathcal{M}_{\text{SW}}^{q < q_0} = 0$
	$\mathcal{M}_{\text{PW}}^{p > p_0} = 1$	$\mathcal{M}_{\text{PW}}^{q > q_0} = \frac{\sqrt{16\kappa^4 - M^2 q^2}}{4\kappa^2}$

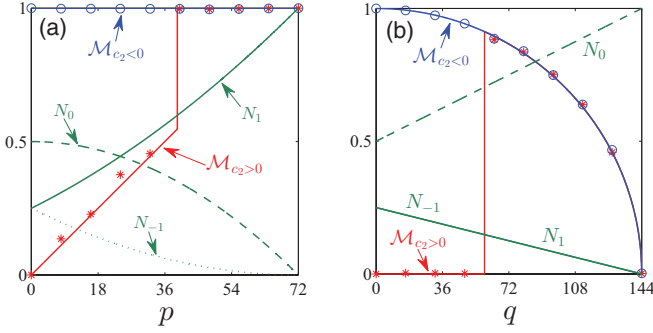


FIG. 4. (Color online) (a) Change in magnetization and atomic distribution of the ground state with the strength of the linear Zeeman field for the cases of  $c_2 = 10$  and  $c_2 = -10$ . (b) Change in magnetization and atomic distribution of the ground state with the strength of the quadratic Zeeman field for the cases of  $c_2 = 10$  and  $c_2 = -10$ . In both (a) and (b), the solid red and blue lines are respectively the corresponding magnetization of  $c_2 > 0$  and  $c_2 < 0$ , which are given by the analytical results shown in Table (I). The green lines represent the atomic numbers  $N_m$ . The red stars and blue circles given by our numerical results are the magnetization for  $c_2 > 0$  and  $c_2 < 0$ , respectively. Moreover, the other parameters in both (a) and (b) are the same:  $\kappa = 6$ ,  $\hbar = M = 1$ , and  $c_0 = 100$ .

$\mathcal{M} = (16\kappa^4 - M^2 q_0^2)^{1/2} / (4\kappa^2)$ , which demonstrates that the phase transition from SW to PW occurs. Again, we have verified these predictions numerically, and the results are summarized in Fig. 4.

To further highlight the effects of Zeeman field on the magnetization of ground state, we map the magnetization vectors onto a sphere with radius  $\mathcal{M} = 1$  as shown in Fig. 5. Before performing the analysis in detail, we introduce the polar angle  $\vartheta = \arctan |\mathcal{M}_+| / \mathcal{M}_z$  and azimuth angle  $\varphi = \arctan \mathcal{M}_y / \mathcal{M}_x$  of the magnetization vector in spherical coordinate frame, where  $\mathcal{M}_+ = \mathcal{M}_x + i\mathcal{M}_y$ . In presence of the external Zeeman field, the polar and azimuth angles of the magnetization vector for the cases of  $c_2 < 0$  and  $c_2 > 0$  are

$$c_2 < 0 : \vartheta = \arctan \frac{\sqrt{2}\alpha_0}{\alpha_1 - \alpha_{-1}}, \varphi = \theta \quad (0 \leq p \leq p_m),$$

$$\vartheta = \frac{\pi}{2}, \quad \varphi = \theta \quad (0 \leq q \leq q_m), \quad (8a)$$

$$c_2 > 0 : \vartheta = \varphi = \text{undefined for } (p = 0) \text{ or } (0 \leq q < q_0),$$

$$\vartheta = 0, \quad \varphi = \text{undefined for } (0 < p < p_0), \quad (8b)$$

$$\vartheta = \arctan \frac{\sqrt{2}\alpha_0}{\alpha_1 - \alpha_{-1}}, \quad \varphi = \theta \text{ for } (p > p_0),$$

$$\vartheta = \frac{\pi}{2}, \quad \varphi = \theta \text{ for } (q > q_0),$$

where  $\theta = \arctan(k_y/k_x)$  is determined by the momentum of ground state. Motivated by the numerical results, we can fix  $\theta = \pi/4$  in the following discussions. Note that, since the SW phase has no magnetization when  $p = 0$  or  $0 \leq q < q_0$ , the polar and azimuth angles of the magnetization vector are undefined in the center of the sphere. Furthermore, as we shall see below, the magnetization of the SW phase is along the  $z$  direction when  $0 < p < p_0$  in a linear Zeeman field, so the azimuth angle of the SW phase is undefined,

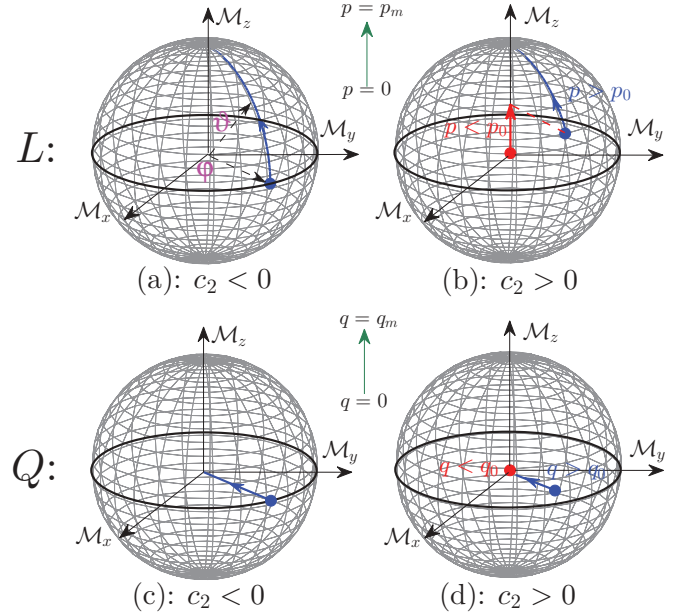


FIG. 5. (Color online) Magnetization vector responds to the linear ( $L$ ) or quadratic ( $Q$ ) Zeeman field. In panels (a)–(d), the red and blue solid circles represent the end of vectors for  $c_2 > 0$  and  $c_2 < 0$ , respectively. Note that the direction of the magnetization vector points to the red or blue circle from the center of the sphere. Furthermore, the red and blue solid lines are the change trajectories of the end of magnetization vectors for SW and PW phases, respectively. In a linear Zeeman field, the end of the vector for  $c_2 > 0$  undergoes a transition from the  $z$  direction to the blue line when  $p > p_0$ . In a quadratic Zeeman field, the end of the magnetization vector for  $c_2 > 0$  undergoes the transition from the center of the sphere to the azimuth angle direction when  $q > q_0$ .

too. Figure 5 shows clearly how the external magnetic field changes the magnetization of the two phases. For the case of  $c_2 < 0$ , the ground state is PW, the linear Zeeman effect rotates the magnetization vector from the transverse direction ( $xy$  plane) to the longitudinal direction ( $z$  direction) along the meridian with azimuth angle  $\varphi = \pi/4$ , but the length of vector is invariant as shown in Fig. 5(a). On the contrary, along the azimuth angle  $\varphi = \pi/4$  direction, the quadratic Zeeman effect demagnetizes the PW in the  $xy$  plane by reducing the length of magnetization vector from one to zero, as shown in Fig. 5(c). For the case of  $c_2 > 0$  summarized in Figs. 5(b) and 5(d), the system would be initially in the SW phase if  $p < p_0$  or  $q < q_0$ . In this case, the length of the magnetization vector in a linear Zeeman field increases linearly along  $z$  direction from zero, but it remains invariant in a quadratic Zeeman field with  $\mathcal{M} = 0$ . While  $p$  (or  $q$ ) surpasses the critical value  $p_0$  (or  $q_0$ ), the SW changes into the PW so that the magnetization vector responds to the Zeeman fields in the same manner as in PW.

## B. Phase diagram and magnetic behaviors of ground state in combined linear and quadratic Zeeman fields

So far, we have focused on the simple case in which the linear and quadratic Zeeman effects are dealt with separately. Experimentally, the linear and quadratic Zeeman effects

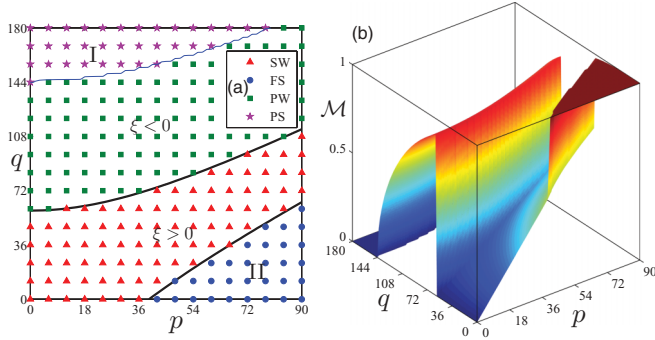


FIG. 6. (Color online) Phase diagram and magnetization distribution for combined effects of linear and quadratic Zeeman fields. In the phase diagram (a), the red triangles, blue circles, green squares, and purple stars respectively denote the SW, zero momentum ferromagnetic state (FS), PW, and zero-momentum polar state (PS) given by the numerical results. The dark line is the phase boundary  $\xi = 0$  between the SW and PW phases, the blue line is the boundary between the PS and PW phases. (b) Magnetization distribution of the system versus  $p$  and  $q$ . In both the panels, the parameters are  $c_0 = 100$ ,  $c_2 = 10$ , and  $\kappa = 6$ .

always coincide with the presence of an external magnetic field. The former can be effectively tuned by changing the total spin of the system, and the latter can usually be tuned by using a linearly polarized microwave field due to the alternating current Stark shift [36,37]. As shown in Refs. [34,35], under a certain range of linear and quadratic Zeeman effects, the ground-state phase diagram of a spin-1 BEC without spin-orbit coupling becomes much richer due to the competition between the linear and quadratic Zeeman effects and the spin-dependent interaction. The typical phase is the broken-axisymmetry state. Therefore, in this subsection we investigate the phase diagram of a spin-1 BEC with spin-orbit coupling in the combination of linear and quadratic Zeeman effects.

We now have a situation similar to the single-particle problem in this combination effect. Since the expression of  $\xi$  is very complex, it is impossible to analytically fix the phase boundary between the SW and PW phases. So we plot the phase diagram and magnetization distribution numerically in Fig. 6 based on the ansatz of Eq. (6). It should be pointed out that for the case of  $c_2 < 0$ , the ground state is always the PW in the whole parameter space  $(p, q)$  due to  $\xi < 0$ . Thus, we just consider the case of  $c_2 > 0$  in following discussions for the sake of simplicity. From the phase diagram in Fig. 6(a), we can see that the ground state initially favors the SW phase when the strengths of the linear and quadratic Zeeman effects are relative weak. However, the PW phase dominates if the quadratic Zeeman effect goes far beyond the linear Zeeman effect. Importantly, our numerical results show that all the atoms are polarized to the state  $\psi_0$  in region I or to the state  $\psi_1$  in region II, respectively. The corresponding order parameters of ground states in these regions are  $\Psi_0 = (0, 1, 0)^T$  and  $\Psi_1 = (1, 0, 0)^T$ . In these states, the momentum of the ground state is zero. All the results above can also be equally reflected by analyzing the magnetization of the system as shown in Fig. 6(b), which shows that the two states  $\Psi_1$  and  $\Psi_0$  are ferromagnetic states with  $\mathcal{M} = 1$  and polar states with  $\mathcal{M} = 0$ , respectively.

Finally, let us consider the possibility of experimentally observing these interesting phenomena. In the previous discussion, all the calculations are performed in arbitrary units which are not related to real experiments. To give some real experimental estimations, we consider a harmonic trapping potential in the form of  $V(r) = \frac{1}{2}M[\omega_\perp(x^2 + y^2) + \omega_z^2 z^2]$ , where  $\omega_\perp$  and  $\omega_z$  represent the transverse and longitudinal trapping potential, respectively. An effective quasi-two-dimensional system can be obtained in the limit of  $\omega_z \gg \omega_\perp$ , and the reduced dimensionless parameters are

$$p_1 = \frac{p}{\hbar\omega_\perp}, \quad q_1 = \frac{q}{\hbar\omega_\perp}, \quad \kappa_1 = \frac{\kappa}{\sqrt{M\hbar\omega_\perp}}, \quad (9a)$$

$$g_0 = \frac{4\pi N(a_0 + 2a_2)}{3\sqrt{2\pi}\zeta_z}, \quad g_2 = \frac{4\pi N(a_2 - a_0)}{3\sqrt{2\pi}\zeta_z}, \quad (9b)$$

where  $\zeta_z = (\hbar/M\omega_z)^{1/2}$ . Note that we have chosen  $\zeta_\perp = (\hbar/M\omega_\perp)^{1/2}$  and  $\hbar\omega_\perp$  as the length and energy scales. According to the real experimental values, we consider  $N = 10^4$   $^{87}\text{Rb}$  atoms in a pancake-shaped harmonic potential with the trapping frequencies  $(\omega_\perp, \omega_z) = (2\pi \times 20\text{Hz}, 2\pi \times 400\text{Hz})$ . In this case, the system parameters  $(\kappa_1, p_1, q_1, g_0, g_2) = (6, 0 \sim 72, 0 \sim 144, 100, 10)$  shown in Figs. 3–6 correspond to the wavelength of Raman lasers  $\lambda \simeq 401.82\text{nm}$  with  $\kappa \propto \hbar/\lambda$ , uniform magnetic field strength  $B \simeq 0 \sim 2.06\text{mG}$ , atomic interactions  $a_0 \simeq 16.27a_B$  and  $a_2 \simeq 22.35a_B$  with  $a_B$  being the Bohr radius. These system parameters are realizable in current experiments.

## V. CONCLUSIONS

Within the framework of mean-field theory, we have systematically investigated the weakly trapped spin-1 Bose-Einstein condensates with spin-orbit coupling in an external Zeeman field and clarified the effects of an external magnetic field on the system. In the single-particle case, the linear and quadratic Zeeman effects play different roles in affecting the structure of the single-particle energy spectrum. When the atomic interactions are taken into account, we give the phase diagram of the mean-field ground state, which is mainly comprised of the magnetized standing-wave phase and plane-wave phase. To develop a physical understanding, we use the linear superposition of two single-particle eigenstates with counterpropagating wave vectors as the variational ansatz to analytically determine the phase boundary between these two phases, which agrees with our numerical results very well. The Zeeman field can induce the phase transition between the standing-wave and plane-wave phases; such phase transition can be further understood by analyzing the response of magnetization of these two phases to an external magnetic field. In particular, when the strength of the Zeeman field surpasses a critical value which is related to the strength of spin-orbit coupling, the system is completely polarized to a ferromagnetic state or a polar state with zero momentum. These investigations not only help to deepen our understanding of the physics behind the interaction between a matter field and gauge field, but also provide an effective way to manipulate the spin-orbit coupled spinor BEC experimentally by using an external magnetic field.

## ACKNOWLEDGMENTS

This work was supported by NCET and the NKBRSC under Grants No. 2011CB921502, No. 2012CB821305, No. 2009CB930701, and No. 2010CB922904, the NSFC under

Grants No. 10934010, No. 11104064, No. 60978019, No. 10901134, No. 10904096, No. 11704175, and No. 11001263, and the NSFC-RGC under Grants No. 11061160490 and No. 1386-N-HKU748/10.

- 
- [1] X. L. Qi and S. C. Zhang, *Phys. Today* **63**, 33 (2010).  
 [2] Y.-J. Lin, R. L. Compton, A. R. Perry, W. D. Phillips, J. V. Porto, and I. B. Spielman, *Phys. Rev. Lett.* **102**, 130401 (2009).  
 [3] Y.-J. Lin, R. L. Compton, K. Jiménez-García, J. V. Porto, and I. B. Spielman, *Nature (London)* **462**, 628 (2009).  
 [4] Y.-J. Lin, K. Jiménez-García, and I. B. Spielman, *Nature (London)* **471**, 83 (2011).  
 [5] Y.-J. Lin, R. L. Compton, K. Jiménez-García, W. D. Phillips, J. V. Porto, and I. B. Spielman, *Nat. Phys.* **7**, 531 (2011).  
 [6] B. M. Anderson, G. Juzeliūnas, V. M. Galitski, and I. B. Spielman, *Phys. Rev. Lett.* **108**, 235301 (2012).  
 [7] Z. Fu, P. Wang, S. Chai, L. Huang, and J. Zhang, *Phys. Rev. A* **84**, 043609 (2011).  
 [8] D. L. Campbell, G. Juzeliūnas, and I. B. Spielman, *Phys. Rev. A* **84**, 025602 (2011).  
 [9] T. D. Stanescu, B. Anderson, and V. Galitski, *Phys. Rev. A* **78**, 023616 (2008).  
 [10] C. Wang, C. Gao, C. M. Jian, and H. Zhai, *Phys. Rev. Lett.* **105**, 160403 (2010); H. Zhai, *Int. J. Mod. Phys. B* **26**, 1230001 (2012).  
 [11] S. Gopalakrishnan, A. Lamacraft, and P. M. Goldbart, *Phys. Rev. A* **84**, 061604 (2011).  
 [12] T.-L. Ho and S. Zhang, *Phys. Rev. Lett.* **107**, 150403 (2011).  
 [13] C. M. Jian and H. Zhai, *Phys. Rev. B* **84**, 060508 (2011).  
 [14] S. K. Yip, *Phys. Rev. A* **83**, 043616 (2011).  
 [15] C. Wu, I. Mondragon-Shem, and X.-F. Zhou, *Chin. Phys. Lett.* **28**, 097102 (2011).  
 [16] S. Sinha, R. Nath, and L. Santos, *Phys. Rev. Lett.* **107**, 270401 (2011).  
 [17] Z. F. Xu, R. Lü, and L. You, *Phys. Rev. A* **83**, 053602 (2011).  
 [18] T. Kawakami, T. Mizushima, and K. Machida, *Phys. Rev. A* **84**, 011607(R) (2011).  
 [19] D. W. Zhang, Z. Y. Xue, H. Yan, Z. D. Wang, and S. L. Zhu, *Phys. Rev. A* **85**, 013628 (2012).  
 [20] R. Barnett, S. Powell, T. Graß, M. Lewenstein, and S. Das Sarma, *Phys. Rev. A* **85**, 023615 (2012).  
 [21] W. Zheng and Z. B. Li, *Phys. Rev. A* **85**, 053607 (2012).  
 [22] Y. Li, L. P. Pitaevskii, and S. Stringari, *Phys. Rev. Lett.* **108**, 225301 (2012).  
 [23] Y. Zhang, L. Mao, and C. Zhang, *Phys. Rev. Lett.* **108**, 035302 (2012).  
 [24] H. Hu, B. Ramachandhran, H. Pu, and X. J. Liu, *Phys. Rev. Lett.* **108**, 010402 (2012).  
 [25] B. Ramachandhran, B. Opanchuk, X. J. Liu, H. Pu, P. D. Drummond, and H. Hu, *Phys. Rev. A* **85**, 023606 (2012).  
 [26] Z. F. Xu, Y. Kawaguchi, L. You, and M. Ueda, *Phys. Rev. A* **86**, 033628 (2012).  
 [27] S. W. Su, I. K. Liu, Y. C. Tsai, W. M. Liu, and S. C. Gou, *Phys. Rev. A* **86**, 023601 (2012).  
 [28] Y. Deng, J. Cheng, H. Jing, C.-P. Sun, and S. Yi, *Phys. Rev. Lett.* **108**, 125301 (2012).  
 [29] T. Ozawa and G. Baym, *Phys. Rev. Lett.* **109**, 025301 (2012); *Phys. Rev. A* **85**, 013612 (2012).  
 [30] J. Radić, T. A. Sedrakyan, I. B. Spielman, and V. Galitski, *Phys. Rev. A* **84**, 063604 (2011).  
 [31] X. Q. Xu and J. H. Han, *Phys. Rev. Lett.* **107**, 200401 (2011).  
 [32] X.-F. Zhou, J. Zhou, and C. Wu, *Phys. Rev. A* **84**, 063624 (2011).  
 [33] T.-L. Ho, *Phys. Rev. Lett.* **81**, 742 (1998); T. Ohmi and K. Machida, *J. Phys. Soc. Jpn.* **67**, 1822 (1998).  
 [34] J. Stenger, S. Inouye, D. M. Stamper-Kurn, H.-J. Miesner, A. P. Chikkatur, and W. Ketterle, *Nature (London)* **396**, 345 (1998).  
 [35] M. Ueda, *Fundamentals and New Frontiers of Bose-Einstein Condensation* (World Scientific, Singapore, 2010); K. Murata, H. Saito, and M. Ueda, *Phys. Rev. A* **75**, 013607 (2007).  
 [36] F. Gerbier, A. Widera, S. Fölling, O. Mandel, and I. Bloch, *Phys. Rev. A* **73**, 041602 (2006).  
 [37] S. R. Leslie, J. Guzman, M. Vengalattore, J. D. Sau, M. L. Cohen, and D. M. Stamper-Kurn, *Phys. Rev. A* **79**, 043631 (2009).